Influence of torsional rigidity of flexible appendages on the dynamics of spacecrafts

Masakatsu Chiba[*] and Hidetake Magata

Department of Aerospace Engineering, Graduate School of Engineering,
Osaka Prefecture University, 1-1 Gakuen-cho, Naka-ku, Sakai, Osaka 599-8531, Japan

Abstract. The influence of torsional rigidity of hinged flexible appendage on the linear dynamics of flexible spacecrafts with liquid on board was analyzed by considering the spacecraft's main body as a rigid tank, its flexible appendages as two elastically supported elastic beams, and the onboard liquid as an ideal liquid. The meniscus of the liquid free surface due to surface tension was considered. Using the Lagrangian of the spacecraft's main body (rigid tank), onboard liquid, and two beams (flexible appendages) in addition to assuming the system moved symmetrically, the coupled system frequency equations were obtained by applying the Rayleigh-Ritz method. The influence of the torsional rigidity of the flexible appendages on the spacecraft's coupled vibration characteristics was primary focus of investigation. It was found that coupled vibration modes especially that of appendage considerably changed with torsion spring parameter κ_t of the flexible appendage. In addition, variation of the main body displacement with system parameters was investigated.

Keywords: hydroelastic vibration; space structure; coupled system; liquid sloshing; zero-gravity; elastic supported; torsional spring

1. Introduction

Because large space structures need to be lightweight, they have low structural rigidity, which causes them to vibrate easily at low frequencies. Thus, thruster injection for attitude control or orbit modification may cause vibrations in flexible appendages, such as antennas and solar arrays, as well as onboard liquids such as wastewater and fuel. This leads to the development of strong coupled vibrations that affect the dynamic behavior of the structure's main body, which pose a serious problem for high-attitude satellites requiring accurate positioning, such as those used for precise astronomical photography. Therefore, clarifying the dynamic interaction behavior of flexible space structures with liquid onboard is crucial for improving space structure stability and reliability.

Several researchers have theoretically examined how liquids slosh in containers in low-gravity environments. For example, Abramson (1996) reviewed studies conducted to that point. Bauer *et al.* (1990a, b) conducted two free vibration analyses of liquids in a cylindrical or rectangular vessel

---

∗Corresponding author, Professor, E-mail: chiba@aero.osakafu-u.ac.jp

(a) Cylindrical tank with two elastically-supported beams
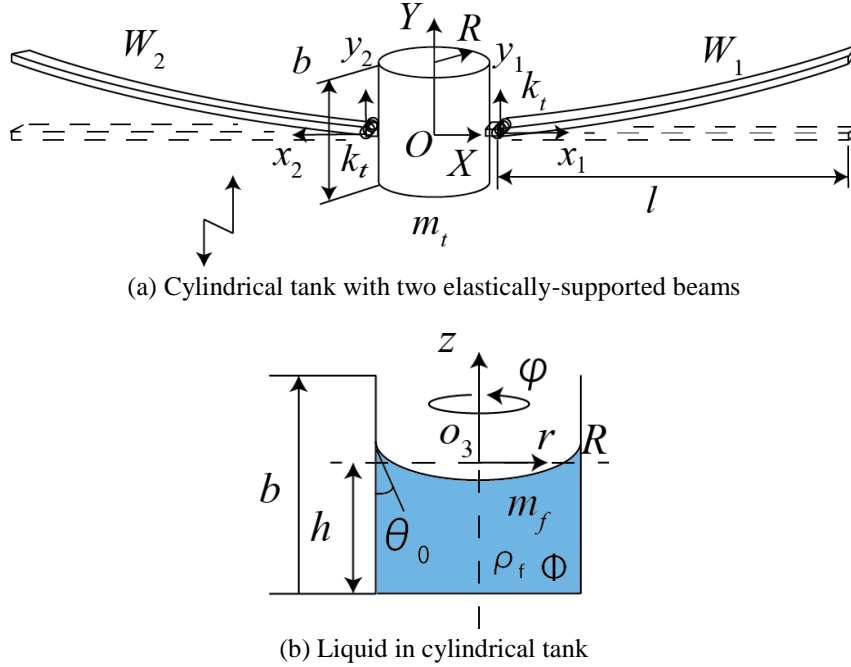

(b) Liquid in cylindrical tank

Fig. 1 Flexible spacecraft model with liquid tank

of the flexible appendages as a torsional spring, and in the third step in this clarification process, we study the spacecraft model that includes the torsional rigidity of the roots of two flexible appendages.

2. Basic equations and boundary conditions

2.1 Analytical model

Fig. 1 shows small amplitude free vibration of a spacecraft with flexible appendages, such as solar arrays, on both sides of the main body, which contains a liquid. In the model, the spacecraft's main body is considered as a rigid cylindrical tank, with two elastically supported elastic beams representing flexible appendages, and a liquid on board. The tank's radius, length, and mass are represented by R, b, and m_t, respectively, and its displacement is represented by Y_M in the inertia coordinate $\mathrm{o}-XY$. The elastic beams are modeled as uniform Euler-Bernoulli beams, each with a length of l, cross-sectional area of A, density of ρ_b, Young's modulus of E, second moment of area of I, and displacements corresponding to $W_1(x_1, t)$ and $W_2(x_2, t)$. The beams are also elastically supported with torsional spring constant k_t. The onboard liquid is treated as an inviscid ideal liquid with a density of ρ_f and a mass of $m_f = \pi R^2 h \rho_f$, where h denotes the height of the liquid when ignoring its meniscus. The liquid's velocity potential, $\Phi(r, \varphi, z, t)$, is given in the coordinate system, $\mathrm{o}-rz\varphi$, which has its origin located on a flat liquid surface. In microgravity, surface

Meniscus of the free surface (represented by Bauer *et al.* 1990b)

$$z_0(r) = \frac{2R\left(1 - \sin^3\theta_0\right)}{3\cos^3\theta_0} - \frac{R}{\cos\theta_0}\sqrt{1 - \left(\frac{r\cos\theta_0}{R}\right)^2} \tag{8}$$

2.2.2 Beams

We modeled the beams with torsional supported mass-free boundary conditions. Therefore, the beam's shearing force at the end, with mass attached, is in balance with the inertia force of the mass. The beam's bending moment is in balance with the moment of the torsional spring (torsional spring constant k_t). In contrast, at the free end, both the shearing force and bending moment are zero

$$x_i = 0: \qquad \text{shearing force:} \qquad -\frac{1}{2}M\ddot{Y}_M(t) - EI\frac{\partial^3 W_i}{\partial x_i^3} = 0 \tag{9}$$

$$\text{bending moment:} \qquad EI\frac{\partial^2 W_i}{\partial x_i^2} - k_t\frac{\partial W_i}{\partial x_i} = 0 \tag{10}$$

$$x_i = l: \qquad \text{shearing force:} \qquad -EI\frac{\partial^3 W_i}{\partial x_i^3} = 0 \tag{11}$$

$$\text{bending moment:} \qquad -EI\frac{\partial^2 W_i}{\partial x_i^2} = 0 \tag{12}$$

2.3 Lagrangian of the system

2.3.1 Lagrangian of the liquid
The Lagrangian of the liquid, L_f, is defined as (see Chiba *et al.* 2017)

$$L_f = \frac{1}{2}m_f\dot{Y}_M^2 + \int_0^R\int_0^{2\pi}\left\{\rho_f\frac{\partial\Phi}{\partial t} - \frac{\sigma}{r}\frac{\partial}{\partial r}\left[r\left\{1 - \left(\frac{r\cos\theta_0}{R}\right)^2\right\}^{3/2}\frac{\partial Z}{\partial r}\right] + \rho_f\ddot{Y}_M(t)z\right\}Z\,r\,dr\,d\varphi \tag{13}$$
$$at\ z = z_0(r)$$

2.3.2 Lagrangian of the beams and main body
The kinetic energies of the beams and main body (tank) are defined as follows

$$T = \frac{1}{2}m_t\dot{Y}_M^2 + \frac{1}{2}\rho_b A\int_0^l\left(\dot{W}_1\right)^2 dx_1 + \frac{1}{2}\rho_b A\int_0^l\left(\dot{W}_2\right)^2 dx_2 \tag{14}$$

The beams and the main body both have potential energy consisting of the stain energy of the beams and the two torsional springs.

$$\frac{\partial \phi}{\partial \eta} = 0 \quad at \ \ \eta = -h_0 \tag{4'}$$

$$\frac{\partial \phi}{\partial \rho} = 0 \quad at \ \ \rho = 1 \tag{5'}$$

$$\frac{\partial \zeta}{\partial \rho} = 0 \quad at \ \ \rho = 1 \tag{6'}$$

$$\int_0^{2\pi} \int_0^1 \zeta\left(\rho, \varphi, \tau\right) \rho d \rho d\phi = 0 \tag{7'}$$

$$\eta_0\left(\rho\right) = \frac{2\left(1 - \sin^3 \theta_0\right)}{3\cos^3 \theta_0} - \frac{1}{\cos \theta_0} \sqrt{1 - \left(\rho \cos \theta_0\right)^2} \tag{8'}$$

2.4.2 Non-dimensionalized boundary conditions for beams

$$\xi_i = 0: \quad \bar{M} \, y_M'' + \frac{\partial^3 w_i}{\partial \xi_i^3} = 0 \, , \quad \frac{\partial^2 w_i}{\partial \xi_i^2} - \kappa_t \frac{\partial w_i}{\partial \xi_i} = 0 \tag{9', (10)'}$$

$$\xi_i = 1: \quad \frac{\partial^3 w_i}{\partial \xi_i^3} = 0, \quad \frac{\partial^2 w_i}{\partial \xi_i^2} = 0 \tag{11', (12)'}$$

2.4.3 Non-dimensionalized Lagrangian
Liquid:

$$\bar{L}_f = \lambda^2 \bar{m}_f \, y_M'^2 + \frac{2\bar{\beta}\bar{\rho}}{\pi\lambda} \int_0^1 \int_0^{2\pi} \left\{ \frac{\partial \phi}{\partial \tau} - \frac{\lambda^3 \gamma}{\bar{\rho}} \frac{1}{\rho} \frac{\partial}{\partial \rho} \left[\rho \left\{ 1 - \left(\rho \cos \theta_0\right)^2 \right\}^{3/2} \frac{\partial \zeta}{\partial \rho} \right] + \lambda y_M'' \eta_0 \right\} \zeta \rho d \rho d\varphi \tag{13'}$$
$$at \ \ \eta = \eta_0(\rho)$$

Rigid tank and beams:

$$\bar{L}_{tb} = \lambda^2 \left\{ \begin{array}{l} \bar{m}_t \, y_M'^2 + \frac{1}{2}\int_0^1 w_1'^2 d\xi_1 + \frac{1}{2}\int_0^1 w_2'^2 d\xi_2 \\[2ex] - \frac{1}{2}\int_0^1 \left(\frac{\partial^2 w_1}{\partial \xi_1^2}\right)^2 d\xi_1 - \frac{1}{2}\int_0^1 \left(\frac{\partial^2 w_2}{\partial \xi_2^2}\right)^2 d\xi_2 - \frac{\kappa_t}{2}\left(\frac{\partial w_1}{\partial \xi_1}\bigg|_{\xi_1=0}\right)^2 - \frac{\kappa_t}{2}\left(\frac{\partial w_2}{\partial \xi_2}\bigg|_{\xi_2=0}\right)^2 \end{array} \right\} \tag{16'}$$

$$\tilde{L}_{tb} = \frac{\Omega}{\pi} \int\limits_0^{2\pi/\Omega} \bar{L}_{tb} d\tau \tag{24}$$

3.2 Liquid velocity potential and liquid surface displacement

The liquid velocity potential, $\bar{\phi}(\rho,\eta)$, which satisfies Eq. (1)' and boundary condition Eqs. (1)' to (8)', and the liquid surface displacement, $\bar{\zeta}(\rho)$, are defined in the following (see Chiba *et al.* 2017)

$$\bar{\phi}(\rho,\eta) = \sum_d A_{0d} J_0(\varepsilon_{0d}\rho) \frac{\cosh\left[\varepsilon_{0d}(\eta+h_0)\right]}{\cosh(\varepsilon_{0d}h_0)} \tag{25}$$

$$\bar{\zeta}(\rho) = \sum_e a_{0e} J_0(\varepsilon_{0e}\rho) \tag{26}$$

where ε_{0d} satisfies the following equations

$$J'_0(\varepsilon_{0d})\left(= -J_1(\varepsilon_{0d})\right) = 0 \tag{27}$$

Substituting Eqs. (25) and (26) into Eq. (20), we calculate the Lagrangian of the liquid as

$$\tilde{L}_f = \lambda^2 \bar{m}_f \Omega^2 \bar{y}_M^2 - \frac{4\bar{\beta}\bar{\rho}}{\lambda} \sum_i \sum_j A_{0j} \varepsilon_{0j} \left(C_{4ji} - C_{5ji}\right) \left[\sum_d A_{0d}\left\{ \Omega^2 \tilde{C}_{1di} + \frac{\lambda^3\gamma}{\bar{\rho}} \varepsilon_{0d} \sum_e (C_{4de} - C_{5de})\tilde{C}_{2ei} \right\} + \lambda\Omega^2 \bar{y}_M \tilde{C}_{3i} \right] \tag{28}$$

where

$$\tilde{C}_{1di} = \frac{C_{1di}}{\chi_{0i}} = \int\limits_0^1 \frac{\cosh\left[\varepsilon_{0d}(\eta_0(\rho)+h_0)\right]}{\cosh(\varepsilon_{0d}h_0)} J_0(\varepsilon_{0d}\rho) J_0(\varepsilon_{0i}\rho)\rho d\rho \tag{29}$$

$$\tilde{C}_{2ei} = \frac{C_{2ei}}{\chi_{0i}} = -\varepsilon_{0i}\varepsilon_{0e} \int\limits_0^1 \rho\left\{1-\left(\rho\cos\theta_0\right)^2\right\}^{3/2} J'_0(\varepsilon_{0e}\rho) J'_0(\varepsilon_{0i}\rho) d\rho \tag{30}$$

$$\tilde{C}_{3i} = \frac{C_{3i}}{\chi_{0i}} = \int\limits_0^1 \eta_0(\rho) J_0(\varepsilon_{0i}\rho)\rho d\rho \tag{31}$$

$$C_{4dn} = \chi_{0n} \int_0^1 \frac{\sinh\left[\varepsilon_{0d}\left\{\eta_0(\rho)+h_0\right\}\right]}{\cosh(\varepsilon_{0d}h_0)} J_0(\varepsilon_{0d}\rho) J_0(\varepsilon_{0n}\rho)\rho d\rho \tag{32}$$

$$C_{5dn} = \chi_{0n} \int_0^1 \frac{\rho\cos\theta_0}{\sqrt{1-\left(\rho\cos\theta_0\right)^2}} \frac{\cosh\left[\varepsilon_{0d}\left\{\eta_0(\rho)+h_0\right\}\right]}{\cosh(\varepsilon_{0d}h_0)} J'_0(\varepsilon_{0d}\rho) J_0(\varepsilon_{0n}\rho)\rho d\rho \tag{33}$$

$$X_{mn}^{00} = \int_0^1 \tilde{w}_m(\xi)\tilde{w}_n(\xi)\,\mathrm{d}\xi = \begin{cases} -\bar{M}\tilde{w}_m(0)\tilde{w}_n(0) & : m \neq n \\ \dfrac{1}{4}\left\{ \tilde{w}_n^2(1) - 3\bar{M}\tilde{w}_n^2(0) + \dfrac{\kappa_t}{\alpha_n^4}\tilde{w}_n'^2(0) \right\} & : m = n \end{cases} \tag{40}$$

$$X_{mn}^{22} = \int_0^1 \frac{\mathrm{d}^2\tilde{w}_m(\xi)}{\mathrm{d}\xi^2}\frac{\mathrm{d}^2\tilde{w}_n(\xi)}{\mathrm{d}\xi^2}\,\mathrm{d}\xi = \begin{cases} -\kappa_t\tilde{w}_m'(0)\tilde{w}_n'(0) & : m \neq n \\ \dfrac{1}{4}\alpha_n^4\left\{ \tilde{w}_n^2(1) - \bar{M}\tilde{w}_n^2(0) + \dfrac{3\kappa_t}{\alpha_n^4}\tilde{w}_n'^2(0) \right\} & : m = n \end{cases} \tag{41}$$

In Eqs. (39) through (41), the dash represents the derivative with respect to ξ.

3.4 Lagrangian of the total system

Finally, we defined the Lagrangian for the entire system as

$$\tilde{L} = \tilde{L}_f + \tilde{L}_{tb}$$

$$= \lambda^2 \left\{ \begin{array}{l} \left(\bar{m}_f + \bar{m}_t\right)\Omega^2 \sum_m \sum_n C_m C_n \tilde{w}_{1m}(0)\tilde{w}_{1n}(0) \\[2mm] - \dfrac{4\bar{\beta}\bar{\rho}}{\lambda^3}\sum_i\sum_j A_{0j}\varepsilon_{0j}\left(C_{4ji} - C_{5ji}\right)\left[\begin{array}{l} \sum_d A_{0d}\left\{\Omega^2\tilde{C}_{1di} + \dfrac{\lambda^3\gamma}{\bar{\rho}}\varepsilon_{0d}\sum_e\left(C_{4de} - C_{5de}\right)\tilde{C}_{2ei}\right\} \\[2mm] + \lambda\Omega^2\,\bar{y}_M\tilde{C}_{3i} \end{array} \right] \\[2mm] + \Omega^2 \sum_m\sum_n C_m C_n X_{mn}^{00} - \sum_m\sum_n C_m C_n X_{mn}^{22} - \kappa_t\sum_m\sum_n C_m C_n \tilde{w}_m'(0)\tilde{w}_n'(0) \end{array} \right\} \tag{42}$$

$$\tilde{\tilde{L}} = \left(\bar{m}_f + \bar{m}_t\right)\Omega^2 \sum_m \sum_n C_m C_n \tilde{w}_{1m}(0)\tilde{w}_{1n}(0)$$

$$- \frac{4\bar{\beta}\bar{\rho}}{\lambda^3}\sum_i\sum_j A_{0j}\varepsilon_{0j}\left(C_{4ji} - C_{5ji}\right)\left[\begin{array}{l} \sum_d A_{0d}\left\{\Omega^2\tilde{C}_{1di} + \dfrac{\lambda^3\gamma}{\bar{\rho}}\varepsilon_{0d}\sum_e\left(C_{4de} - C_{5de}\right)\tilde{C}_{2ei}\right\} \\[2mm] + \lambda\Omega^2\,\bar{y}_M\tilde{C}_{3i} \end{array} \right] \tag{43}$$

$$+ \Omega^2 \sum_m\sum_n C_m C_n X_{mn}^{00} - \sum_m\sum_n C_m C_n X_{mn}^{22} - \kappa_t\sum_m\sum_n C_m C_n \tilde{w}_m'(0)\tilde{w}_n'(0)$$

3.5 Rayleigh-Ritz method

We then applied the *Rayleigh-Ritz* method to obtain the following minimalized condition for $\tilde{\tilde{L}}$:

$$\frac{\partial\tilde{\tilde{L}}}{\partial A_{0j}} = 0,\ \frac{\partial\tilde{\tilde{L}}}{\partial B_m} = 0 \tag{44}$$
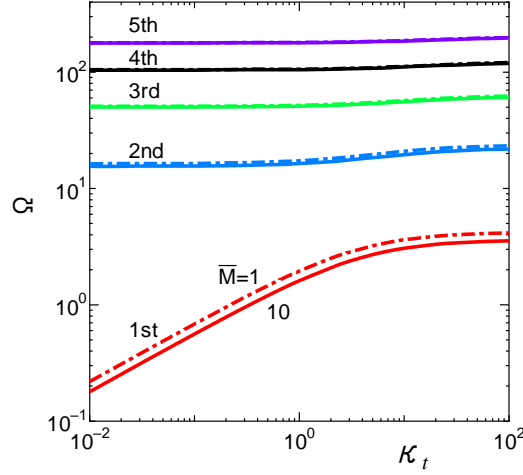
Fig. 2 Natural circular frequency with torsional spring parameter κ_t (without liquid: $\bar{M} = 1, 10$)

(a) $\kappa_t = 0.01$ (b) $\kappa_t = 0.1$ (c) $\kappa_t = 1$ (d) $\kappa_t = 10$ (e) $\kappa_t = 100$
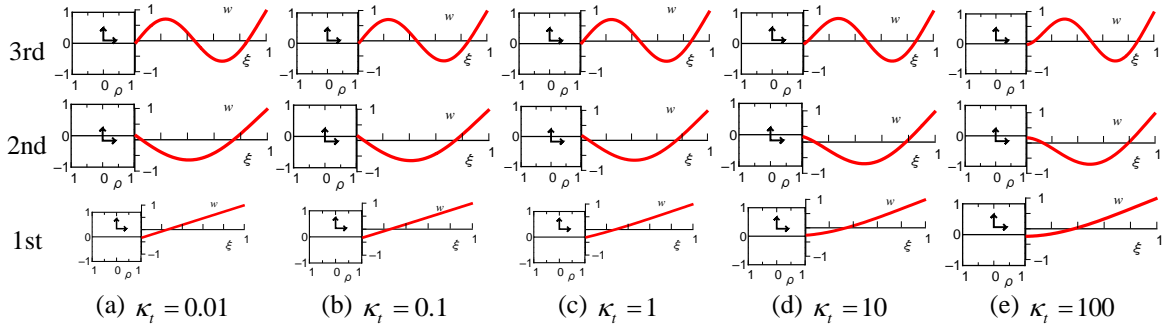
Fig. 3 Vibration mode with torsional spring parameter κ_t (without liquid: $\bar{M} = 1$); (a) κ_t=0.01; (b) κ_t=0.1; (c) κ_t=1; (d) κ_t=10; (e) κ_t=100

4.1.1 Influence of κ_t on natural circular frequency

Fig. 2 shows the natural circular frequency variations of the lowest five modes with κ_t. Because κ_t is defined as $\kappa_t = k_t l / EI$, an increase in κ_t corresponds to an increase in the torsional spring constant (keeping the beam's length, l, constant), or an increase in beam length, l, (keeping κ_t constant). In the figure, solid and single-dotted lines correspond to results for $\bar{M} = 10$ and 1, respectively. We found that as κ_t increases, the natural circular frequencies also increase and tend to the values when the beam is clamped ($\Omega = 3.52,\ 22.03,\ 61.70$ when $\bar{M} \to \infty$) (see, Chiba *et al.* 2017).

4.1.2 Influence of κ_t on vibration mode

Fig. 3 shows the lowest three vibration modes for κ_t=0.01, 0.1, 1, 10, 100 when $\bar{M} = 1$. In Fig. 3, a square indicates the spacecraft's main body (cylindrical tank), the red curve indicates the right-hand side beam's vibration mode, the crossing point of the two small arrows indicates the inertia frame origin, and the distance of the crossing point from the tank's center indicates the tank's displacement. In addition, the displacements of tank y_M and beam w are normalized such that their maximum of which is unity.
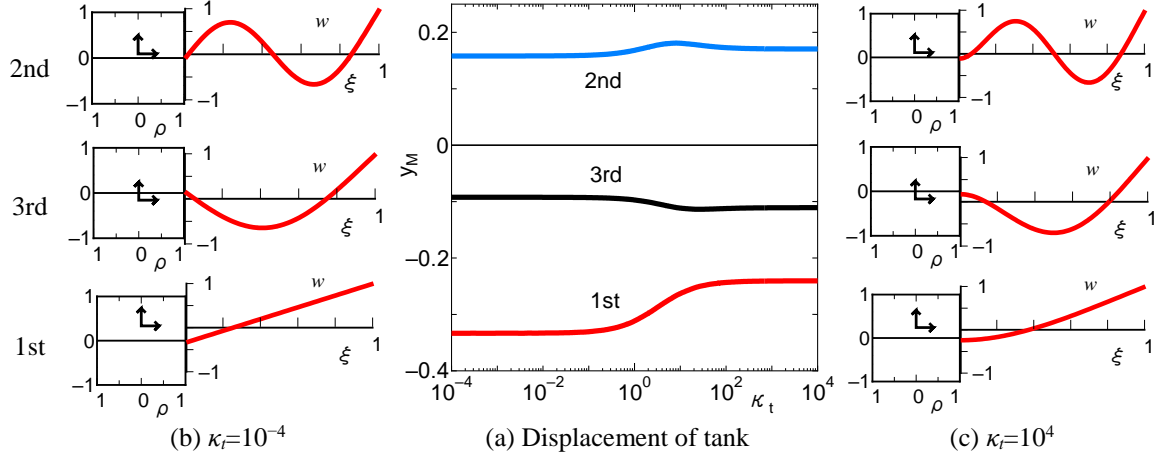
Fig. 4 Variation of displacement of tank y_M and vibration mode with torsional spring parameter κ_t (without liquid $\bar{M}=1$)

motion is predominant, whereas the tank moves in a coupled vibration in which beam vibration is predominant.

4.2.4 Variation of natural frequency with liquid height

Fig. 8 shows natural circular frequency variations with liquid height h_0 when $\theta_0=60°$, $90°$, $100°$ ($\bar{\rho}=1$, $\gamma=10^{-4}$, $\bar{\beta}=10$, $\lambda=10$, $\bar{m}_t=1$, $\kappa_t=1$). The frequency curve with a dashed line corresponds to the coupled frequency where beam motion is predominant, whereas curves with solid lines correspond to coupled frequencies in which the liquid mode is predominant. As h_0 decreases, these two frequency curves cross.

4.2.5 Influence of liquid height on the displacement of tank

Fig. 9 shows tank displacement y_M variations with liquid height h_0 for three contact angles, $\theta_0=60°$, $90°$, $100°$, which correspond to the first and second modes when $\kappa_t=1$. Single-dotted vertical lines correspond to the h_0 value in which two natural frequency curves cross. We found that displacement y_M drastically changes near the crossing region when $\theta_0=60°$ and $100°$ in the vibration mode in which liquid sloshing is predominant. When the κ_t value is small, i.e., $\kappa_t=1$, the liquid fuel is consumed throughout the spacecraft's mission. Additionally, the two types of coupled frequencies, especially those with the lowest sloshing modes, approach each other, producing movement of the main body (tank).

5. Conclusions

The influence of the torsional rigidity of the hinged flexible appendage on the dynamics of liquid-containing flexible space structures was analyzed by considering a spacecraft's main body as a rigid tank, its flexible appendages as two elastically supported elastic beams, and the liquid on board as an ideal liquid, considering the meniscus of the liquid free surface. The obtained results are summarized as follows:
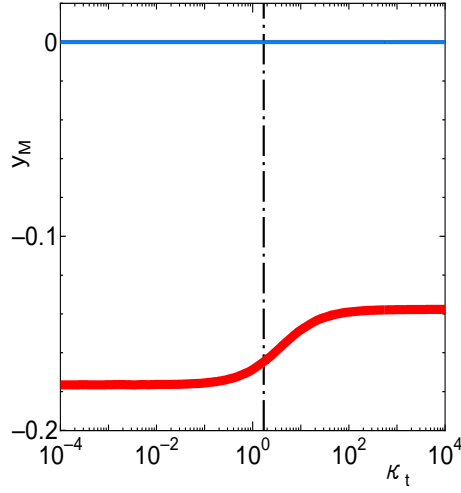
Fig. 7 Displacement of tank y_M with torsional spring parameter κ_t: $\theta_0 = 90°$, $h_0 = 1$, $\bar{\rho} = 1$, $\gamma = 10^{-4}$, $\bar{\beta} = 10$, $\lambda = 10$, $\bar{m}_t = 1$

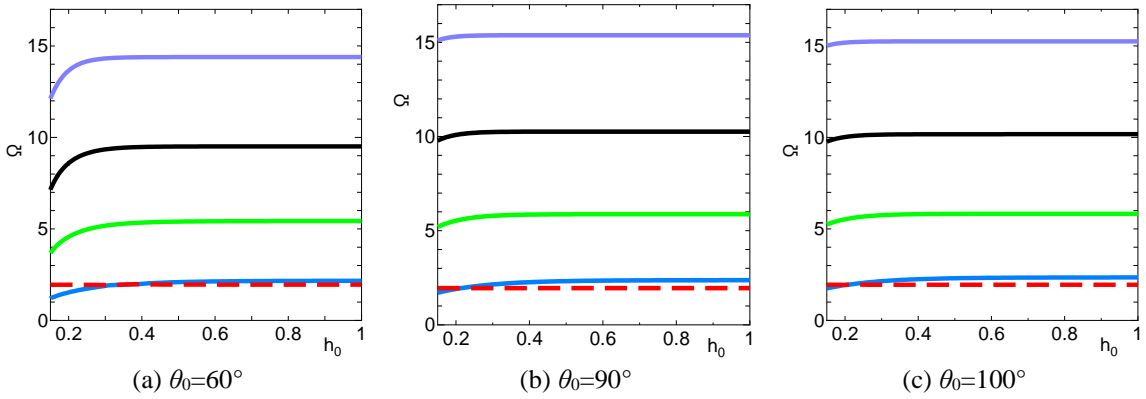(a) $\theta_0 = 60°$ (b) $\theta_0 = 90°$ (c) $\theta_0 = 100°$

Fig. 8 Natural circular frequency with liquid height h_0: $\bar{\rho} = 1$, $\gamma = 10^{-4}$, $\bar{\beta} = 10$, $\lambda = 10$, $\bar{m}_t = 1$, $\kappa_t = 1$
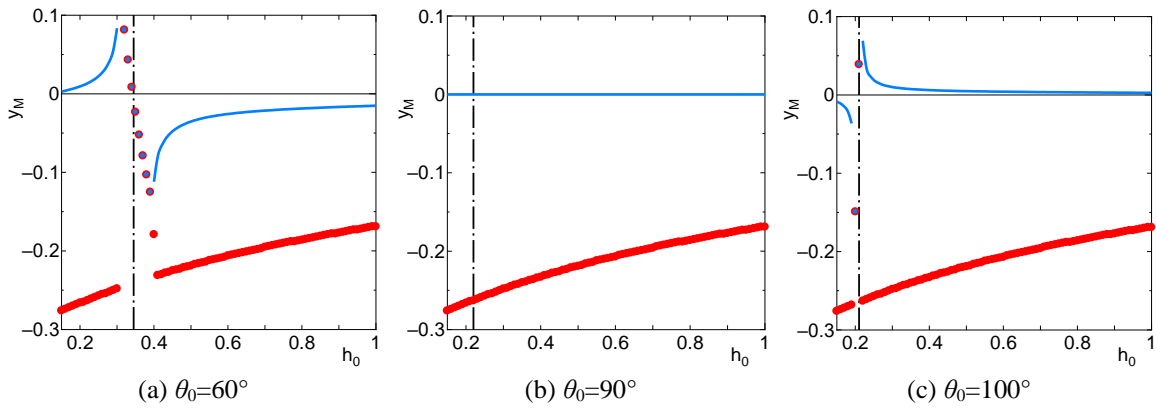

(a) $\theta_0 = 60°$ (b) $\theta_0 = 90°$ (c) $\theta_0 = 100°$

Fig. 9 Displacement of tank y_M with liquid height h_0: $\bar{\rho} = 1$, $\gamma = 10^{-4}$, $\bar{\beta} = 10$, $\lambda = 10$, $\bar{m}_t = 1$, $\kappa_t = 1$

Li, Q., Ma, X. and Wang, T. (2011), "Equivalent mechanical model for liquid sloshing during draining", *Acta Astronaut.*, **68**(1-2), 91-100.

McIntyre, J.E. and McIntyre, J.M. (1982), "Some effects of propellant motion on the performance of spinning satellites", *Acta Astronaut.*, **9**(12), 645-661.

Santini, P. and Barboni, R. (1978), "Motion of orbiting spacecrafts with a sloshing fluid", *Acta Astronaut.*, **5**(7-8), 467-490.

Santini, P. and Barboni, R. (1983), "A minicomputer finite elements program for microgravity hydroelastic analysis", *Acta Astronaut.*, **10**(2), 81-90.

Utsumi, M. (2004), "A mechanical model for low-gravity sloshing in an axisymmetric tank", *Trans. ASME, J. Appl. Mech.*, **71**(5), 724-730.

Young, T. and Baozeng, Y. (2017), "Simulation of large-amplitude three dimensional liquid sloshing in spherical tanks", *AIAA J.,* **55**(6), 2052-2059.

Yuanjun, H., Xingrui, M., Pigping, W. and Benli, W. (2007), "Low-gravity liquid nonlinear sloshing analysis in a tank under pitching excitation", *J. Sound Vibr.*, **299**(1-2), 164-177.

Zhou, Z. and Huang, H. (2015), "Constraint surface model for large amplitude sloshing of the spacecraft with multiple tanks", *Acta Astronaut.*, **111**, 222-229.

CC

Nomenclature (Non-dimensional)

A	Beam cross-sectional area
b	Tank length
E	Young's modulus of beam
h	Equivalent liquid height : $\left(h_0 = h / R\right)$
I	Beam second moment of area
k_t	Torsional spring constant $\left(\kappa_t = k_t l / EI\right)$
l	Beam length $\left(\lambda = l / R\right)$
m_f	Liquid mass : $(\bar{m}_f = m_f / 2\rho_b Al)$
m_t	Rigid tank mass : $(\bar{m}_t = m_t / 2\rho_b Al)$
M	Total of m_f and m_t : $(\bar{M} = \bar{m}_f + \bar{m}_t)$
$O - XY$	Spacecraft coordinate system
$\text{o} - r\varphi z$	Tank coordinate system : $(\text{o} - \rho\varphi\eta)$

R Tank radius

t Time: $(\tau = \omega_b t)$

Y_M Rigid tank displacement: $(y_M = Y_M / l)$

$W_i(x_i, t)$ Beam displacements: $(w_i = W_i / l)$

$Z(r, \varphi, t)$ Liquid surface displacement: $(\zeta = Z / R)$

$z_0(r)$ Static liquid free surface: $(\eta_0 = z_0 / R)$

$Z_f(r, \varphi, t)$ Liquid free surface displacement

$\Phi(r, \varphi, z, t)$ Liquid velocity potential: $(\phi = \Phi / \omega_b R^2)$

$\bar{\beta}$ Beam and tank area ratio $(= \pi R^2 / 2A)$

θ_0 Static contact angle of liquid

ρ_f Liquid density

ρ_b Beam density

σ Coefficient of free surface tension: $(\gamma = \sigma R^2 l / EI)$

$\bar{\rho}$ Density ratio $(= \rho_f / \rho_b)$

ξ_i Non-dimensional coordinate: $(= x_i / l)$

ω Coupled natural circular frequency $(\Omega = \omega / \omega_b)$

ω_b Natural circular frequency parameter $(= \sqrt{EI / \rho_b A l^4})$